K. McDonald
Princeton U.
Jan. 3, 1997

E-144: Comparison of Methods of Reconstruction of Nonlinear Compton Scattering via ECAL Data

Abstract

This note compares and contrasts the approaches of Glenn Horton-Smith and Kostya Shmakov to extracting the spectra of nonlinear Compton scattering from the data recorded with the ECAL Si-W calorimeter. This note is based in part on Glenn's note "ECAL 'Best Aperture' Reconstruction" (Sept. 29, 1995), and Kostya's draft sections for the Phys. Rev. paper, as well as conversations with Glenn and Kostya.

1 Introduction

1.1 Coordinates, Indices and ECAL Segmentation

The FFTB dump magnets disperse the Compton scattered electrons vertically which we will call the y direction. The is therefore a correlation between an electrons momentum and the y-coordinate at which the electron enters the ECAL. The Compton scattering spectrum is a rapid and monotonic function of y.

The ECAL (see Fig. 1) is segmented into horizontal rows which I will label by subscript i. Usable signal can be found in only the top four rows – and we must decide later to what extent we trust the data in the fourth row where backgrounds are very high. Typically signals in row 4 are of order 1% of those in row 1.

The ECAL is segmented vertically into four columns, often grouped as 'inner' and 'outer'. The ECAL is segmented longitudinally into four segments. The last segment contains little signal from electrons that enter the front of the ECAL.

In Kostya's analysis the first three longitudinal segments are summed. Kostya also groups the two inner columns together, and the two outer columns together. In contrast, Glenn keeps the data from every segment of ECAL separate, and extends the row index i to cover all types of segments. I will try to remind the reader when the slightly different use of index i by Glenn and by Kostya is important.

1.2 ECAL Calibrations and Response Kernels

Extensive studies of ECAL performance have been made in parasitic runs of the FFTB. Pulses of 1-100 electrons were obtained at a selected momentum in the range 5-30 GeV. The beam-spot size was about 1 mm. The vertical position of the ECAL varied in small steps.

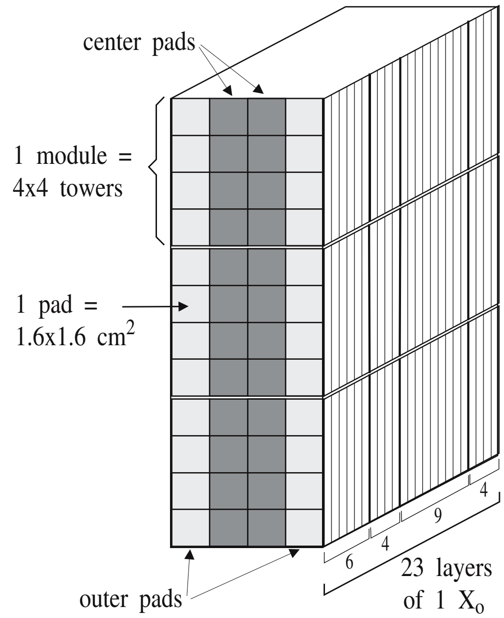

Figure 1: Segmentation of the ECAL calorimeter.

1.2.1 ECAL Response Functions $X_i(y)$

In this way the energy response of any ECAL segment i to an electron entering the front of ECAL at height y with energy E was determined. The fractional (or normalized) response, $X_i(y, E)$, for a given geometrical configuration was found to be reasonably independent of energy in the range 5-30 GeV. Hence we summarize calibration data with the energy-independent response $X_i(y)$, where the normalization condition is

$$\sum_i X_i(y) = 1, \tag{1}$$

if y is not too near the edge of the calorimeter. *(Do we need a remark about special treatment for y near the top of ECAL?)*

In Kostya's analysis longitudinal segment 4 is ignored and the signals in segments 1-3 added. He also groups the horizontal segments in a given row into a logical inner segment I consisting of the two inner physical segments, and a logical outer segment O consisting of the two outer physical segments.

Further, Kostya chooses the ADC gain conversion constant so that the energy deposited by an electron in the inner segments is called 100% of the electron's energy. That is,

$$\sum_i X_{I,i}(y) = 1, \tag{2}$$

where subscript I refers to the inner segments.

The ECAL calibrations revealed that the ratio of the energy deposited in the outer segments to that deposited in the inner segments is 0.0713. Therefore,

$$\sum_i X_{O,i}(y) = 0.0713. \tag{3}$$

Figure 2 shows that calibration data for response functions X_I and X_O, along with fits described below.

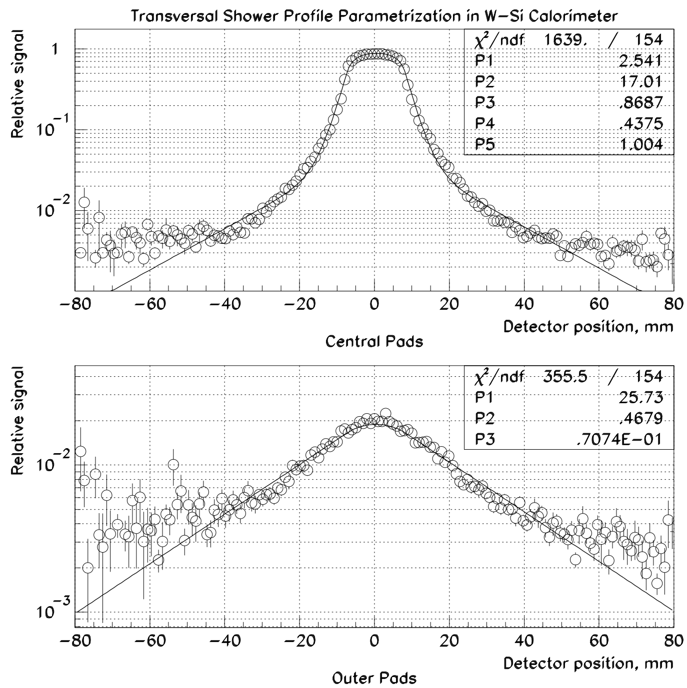

Figure 2: Top: the response function $X_I(\Delta y)$ for inner columns of the ECAL, summed over longitudinal segments 1-3. Bottom: function $X_O(\Delta y)$ for outer columns. Circles = data; curve = calculation based on eq. (7).

1.2.2 The Response Kernels $K_i(y, y')$

Guided in part by EGS simulations, Kostya further analyzed the calibration data to extract what he calls the response kernel $K_i(y, y')$, where an electron enters the ECAL at height y and deposits fractional energy $K/1.0713$ in a horizontal slice at height y' within segment i. To a good approximation the kernel depends on positions y and y' only through the absolute value of their difference: $|y - y'|$. The factor $1/1.0713$ in the definition of K arises from Kostya's convention that the channel gains are adjusted until the nominal energy deposited in the inner segments is exactly the incident energy, and the nominal energy deposited in inner + outer segments is 1.0713 times the incident energy.

There is not a separate kernel for each segment i, but one functional form for each class of segments that differ only by row number. In particular, all segments in inner columns have kernels of the form

$$K_I(y, y') = \frac{w \exp(-|y - y'|/b_1)}{2b_1} + \frac{(1 - w)\exp(-|y - y'|/b_2)}{2b_2}, \tag{4}$$

and all segments in outer columns have kernels of form

$$K_O(y,y') = 0.0713\frac{\exp(-|y-y'|/b_3)}{2b_3}. \tag{5}$$

In Kostya's analysis, $b_1 = 1.940$, $b_2 = 9.561$,$b_3 = 16.908$ and $w = 0.703$. For Glenn's analysis the coefficients b and w vary with longitudinal segment, and each kernel has an overall normalization factor less than 1.

The kernels are normalized (by Kostya) to

$$\int K_I(y,y')dy' = 1, \qquad \text{while} \qquad \int K_O(y,y')dy' = 0.0713. \tag{6}$$

The segment response data, $X_i(y)$, can now be represented in terms of an integral over the response kernel. Thus

$$X_i(y) = \int_{y_i}^{y_{i+1}} K_i(y,y')dy', \tag{7}$$

where row i spans the interval $[y_i, y_{i+1}]$. The normalization conditions (2) and (3) are satisfied in view of eq. (6). Figure 2 shows curves based on eq. (7).

1.3 Backgrounds

Signal electrons can only enter the front of the inner columns. However, many Compton-scattered electrons initiate showers in the beampipe and other shielding above the ECAL, causing a spray of electrons and photons into the top and back of ECAL. This is the principal type of background in the ECAL, and it is called 'splash' within the E-144 group.

There also exists electronic crosstalk at the level of a few percent between various segments of the ECAL.

The 'splash' background has been characterized by Glenn using x-t scans (E-144 Collaboration Meeting, Sept. 1995). The key insight is that splash is largely due to showers initiated by $n = 1$ Compton scattered electrons.

When ECAL is positioned to detect nonlinear Compton scattering of $n \geq 2$ this signal is very sensitive to the time offset between the electron and laser pulses. However, the $n = 1$ scattering signal is much less sensitive. Thus as a time offset is introduced there is a region in which the $n < 2$ scattering has vanished but substantial $n = 1$ signal remains. Corresponding to the latter is 'splash' detected by the ECAL. *Show a figure here.* In this way the pattern of splash over ECAL segments can be determined.

In Kostya's analysis the ratio of the splash background in the inner segments of row i to that in the outer segments is called L_{ii}. This ratio is is largest when ECAL is positioned close to the electron beam, and hence close to the trajectories of $n = 1$ Compton-scattered electrons.

Figure 3 shows the L_{ii}. To a first approximation the 'splash' ratio L is only a function of the y-coordinate of the ECAL row.

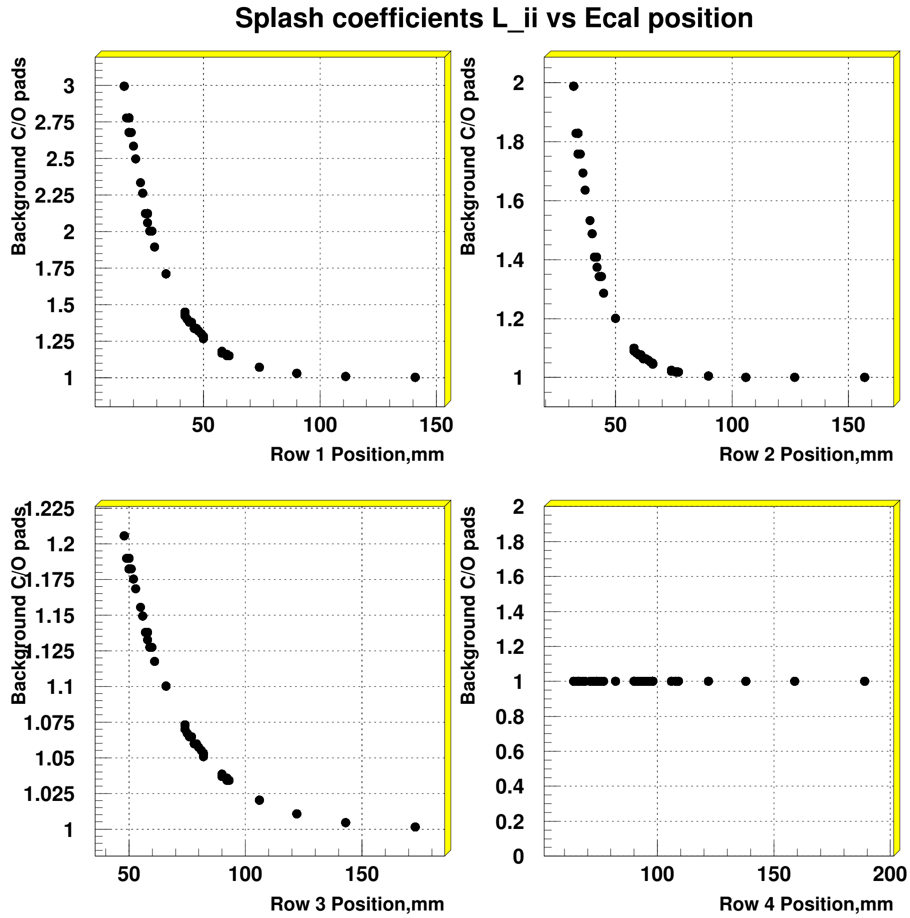

Figure 3: The 'splash' coefficients L_{ii} as function of ECAL vertical position.

2 The Main Analysis Algorithms

The nonlinear Compton Scattering process produces an energy spectrum $f(y)$ of scattered electrons hitting the ECAL at height y. Because of fluctuations in the e-laser overlap this spectrum varies from pulse to pulse. The general strategy is to reconstruct the spectrum f for each pulse and then sum over pulses.

Of course, we cannot fully reconstruct a continuous spectrum such as f from data in a detector with a finite number of segments. Rather, what we desire to reconstruct is the integral F_i of the spectrum f over segment i:

$$F_i = \int_{y_i}^{y_{i+1}} f(y')dy'. \tag{8}$$

The energy D_i observed in segment i during some pulse is related to the Compton spectrum f by

$$D_i = \int dy f(y) \int_{y_i}^{y_{i+1}} K_i(y, y') dy' = \int dy f(y) X_i(y), \tag{9}$$

recalling eq. (7).

2.1 Overview of the Methods

2.1.1 Kostya

Kostya's approach is to determine for each pulse a matrix M_{ij} such that the observed data D_i is related to the desired spectrum F_i by

$$D_i = \sum_j M_{ij} F_j, \tag{10}$$

and then invert this matrix to yield

$$F_i = \sum_j R_{ij} D_j, \qquad \text{where} \qquad R_{ij} = M_{ij}^{-1}. \tag{11}$$

The matrix M_{ij} is found by an iterative process described in sec. 2.4.1 below in which the integrals (9) are performed analytically for a 'polyline' approximation to spectrum f derived from the F_i of the previous iteration. The initial hypothesis is that $F_i = D_i$. Only two iterations are used to find the reconstructed F_i.

In Kostya's approach index i runs from 1 to 4, corresponding to the top four rows of ECAL.

2.1.2 Glenn

Glenn's approach is based on the observation that the desired reconstruction (11) can be combined with eq. (9) to write

$$F_i = \sum_j R_{ij} D_j = \int dy f(y) \sum_j R_{ij} X_j(y) = \int dy f(y) g_i(y), \tag{12}$$

where

$$g_i(y) = \sum_j R_{ij} X_j(y). \tag{13}$$

Comparing eq. (13) with eq. (8) we see that the g_i (called 'aperture functions' by Glenn) should obey

$$g_i(y) = \begin{cases} 1, & y_i < y < y_{i+1}, \\ 0, & \text{otherwise.} \end{cases} \tag{14}$$

Glenn finds the matrix elements R_{ij} for a given geometric configuration of ECAL and shielding by a χ^2-minimization process involving the g_i. Briefly

$$\chi^2 = \sum_{i,k} \frac{\left(\sum_j R_{ij} X_j(y_k) - g_i(y_k)\right)^2}{\sigma_{ik}^2}, \tag{15}$$

where the deviates are evaluated at y_k spaced 1 mm apart. Some art in choosing the 'errors' (or tolerances) σ_{ik} is required, as discussed further in sec. 2.4.2.

In Glenn's approach index i runs over all segments of ECAL.

A sense of how well the procedure works is given in Fig. 4, which shows the aperture functions g_i for four rows in ECAL.

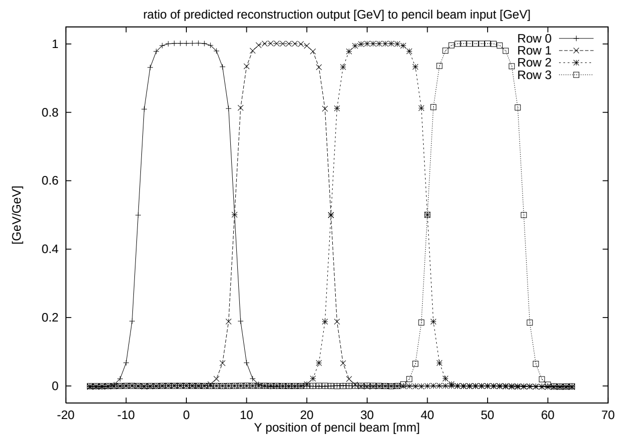

Figure 4: The aperture functions defined by eq. (13) for the top four rows of ECAL. *(What longitudinal segments are involved?)*

2.1.3 Remark

In the absence of background the analyses of Glenn and Kostya proceed by somewhat different paths to arrive at the common goal, eqs. (11) and (12). To help show the commonality of the approaches it would be extremely interesting if Kostya's M_{ij}^{-1} could be used to evaluate the four aperture functions g_i defined by eq. (13). *(Since matrix M_{ij} varies slightly from event to event this should be done for a number of events and the results superimposed. I predict that Kostya's approach would produce results very similar to those in Fig. 4.)*

2.2 Overview of the Background Subtraction Techniques

(It would be good to have a figure that gives a sense of typical signal sizes in the inner and outer segments of the top 4 rows of ECAL.)

2.2.1 Kostya

As noted in sec. 1.3, about 93% of the energy from Compton-scattered electrons is deposited in the inner columns of ECAL. However, energy from background processes in more uniformly divided between the inner and outer columns. Kostya's background subtraction method is an extension of the simple prescription that the Compton signal could be obtained by subtracting the energy in the outer segments from that in the inner segments.

Let S designate energy deposited from Compton-scattered electrons entering the front of ECAL and B that deposited by the background processes (predominantly 'splash' from scattered electrons that hit shielding rather than the front of ECAL). Then the observed energy D_I in the inner columns can be written as a vector with index i suppressed:

$$D_I = D_{I,S} + D_{I,B}. \tag{16}$$

We introduce vector D_O as the observed energy in the outer columns of ECAL. This is, of course, partly due to the small leakage from electrons that enter the front of ECAL and partly due to 'splash' energy. So we write

$$D_O = D_{O,S} + D_{O,B}. \tag{17}$$

Just as the Compton signal $D_{I,S}$ in the inner segments can be related to the Compton spectrum vector F by eq. (10) rewritten as

$$D_{I,S} = MF, \tag{18}$$

in terms of matrix M, there exists a matrix N such that the Compton leakage signal $D_{O,S}$ in the outer segments is related by

$$D_{O,S} = NF. \tag{19}$$

Details of matrix N will be given in sec. 2.4.1 below.

The key to the background subtraction is that we can relate the background energy in the inner segments to that in the outer segments according to

$$D_{I,B} = LD_{O,B}, \tag{20}$$

where matrix L is diagonal, with diagonal elements that can be determined from x-t scans as described in sec. 1.3.

Once matrices L and N are known the analysis is readily completed. The observed energy in the inner segments can now be written

$$D_I = D_{I,S} + D_{I,B} = MF + LD_{O,B}, \tag{21}$$

while that in the outer segments is

$$D_O = D_{O,S} + D_{O,B} = NF + D_{O,B}. \tag{22}$$

On subtracting L times eq. (22) from eq. (21) and noting eq. (20) we have

$$D_I - LD_O = [M - LN]F, \tag{23}$$

and hence

$$F = [M - LN]^{-1}(D_I - LD_O). \tag{24}$$

2.2.2 Glenn

In Glenn's approach the background energy in segment i is written as B_i. We note that the background in dominated by showers of $n = 1$ Compton scatters (rather than nonlinear Compton scatters) so we expect that vector B_i varies from event to event only in overall normalization. The relative values of B_i can be determined from x-t scans. *(Again, I don't know exactly how this is done; the full writeup should include an explanation of this key point.)*

The reconstruction matrix R_{ij} introduced in eqs. (11) and (12) should produce no signal when applied to the background vector:

$$\sum_j R_{ij} B_j = 0. \tag{25}$$

This condition is enforced during the determination of the R_{ij} by adding a term to the χ^2:

$$\chi^2 = \sum_{i,k} \frac{\left(\sum_j R_{ij} X_j(y_k) - g_i(y_k)\right)^2}{\sigma_{ik}^2} + \frac{\left(\sum_j R_{ij} B_j\right)^2}{\sigma'^2}, \tag{26}$$

where the tolerance σ' must also be judiciously chosen.

2.2.3 Remarks

We can get a sense of how Glenn's and Kostya's subtraction methods are related by recalling that Glenn's index i runs over all segments, but Kostya's does not.

First I imagine that Glenn's analysis summed over longitudinal segments just like Kostya's. *(I may be wrong but I think this is a benign assumption.)* Further, I restrict Glenn's analysis to the top 4 rows of ECAL. *(This also is benign as these is essentially no signal in the lower rows.)* Then Glenn's i would run from 1 to 8, 1-4 being the inner pads of the top 4 rows, and 5-8 being the outer pads of the top 4 rows.

In this approximation I can write Glenn's data vector D_{Glenn} as being made up of Kostya's vectors $D_{I,Kostya}$ and $D_{O,Kostya}$ according to

$$D_{Glenn} = \begin{bmatrix} D_{I,Kostya} \\ D_{O,Kostya} \end{bmatrix}. \tag{27}$$

Likewise the background vectors could then be related by

$$B_{Glenn} = \begin{bmatrix} L D_{O,B,Kostya} \\ D_{O,B,Kostya} \end{bmatrix}. \tag{28}$$

We see that the diagonal elements of Kostya's (diagonal) matrix L should simply the ratios of certain elements of Glenn's background vector. Thus $L_{11} = B_1/B_5$, *etc. (It would be good to check how well these relations are satisfied in practice.)*

The reconstructed spectrum should be related by

$$F_{Glenn} = \begin{bmatrix} F_{Kostya} \\ 0 \end{bmatrix}, \tag{29}$$

since there should be no Compton signal incident on the outer pads.

Hence the translation of Kostya's eq. (24) into Glenn's form (12) is

$$F_{Glenn} = R_{Glenn} D_{Glenn} = \begin{bmatrix} [M - LN]^{-1} & -[M - LN]^{-1} L \\ 0 & 0 \end{bmatrix} \cdot \begin{bmatrix} D_{I,Kostya} \\ D_{O,Kostya} \end{bmatrix}. \tag{30}$$

We see that Glenn's eq. (25) is automatically satisfied in Kostya's analysis:

$$R_{Glenn} B_{Glenn} = \begin{bmatrix} [M - LN]^{-1} & -[M - LN]^{-1} L \\ 0 & 0 \end{bmatrix} \cdot \begin{bmatrix} L D_{O,B,Kostya} \\ D_{O,B,Kostya} \end{bmatrix} = 0. \tag{31}$$

That is, the analysis matrix R that takes the observed data D into the underlying Compton spectrum F also takes the background into the null vector. The reaffirms that the main difference between Glenn's and Kostya's approach is in their procedures to calculate matrix R.

2.3 Overview of Error Estimates

Statistical error related directly to the number of electrons hitting the ECAL are calculated by Christian's program that further processes the results of Glenn's and Kostya's analyses. The latter analyses assign errors that represent the systematic uncertainty in the analysis procedures due to limitations of the numerical algorithms.

2.3.1 Kostya

Kostya's analysis uses an iterative procedure to unfold the Compton spectrum F_i starting from an initial hypothesis. Hence it is easy to check how well this procedure works by generating trial data from a known hypothesis $f(y)$, calculating both the corresponding ideal spectrum F_i and the 'observed' data D_i, and finally reconstructing a spectrum F_i' from the D_i. This is done in the presence of some model background as well.

We could then repeat this check for a reasonable class of trial spectra $f(y)$ and accumulate error estimates:

$$\sigma_i^2 = \langle (F_i - F_i')^2 \rangle. \tag{32}$$

I gather that a procedure like this is used to estimate the error on results from row 1, but not for the other rows. The result of the study was that $\sigma_1/F_1 \approx 0.05$.

Rather, Kostya notes that the data in a lower row is heavily influenced by feeddown from the rows above, given that the Compton spectrum is steeply falling. He therefore argues that the biggest uncertainty in row j is the uncertainty in the feeddown from rows with $i < j$. In this way he propagates the uncertainty in row j all the way back to that in row 1.

To keep track of the feeddown Kostya argues as follows:

$$F_i = \sum_j (M - LN)^{-1} D_I - \sum_j (M - LN)^{-1} L D_O, \tag{33}$$

according to eq. (24). He then supposes that the relative error on each of these terms is just σ_1/F_1, which is justified to the extent that feeddown from row 1 dominates (or that the relative error is the same everywhere). Then

$$\sigma_i = \frac{\sigma_1}{F_1}\sqrt{\left[\sum_j (M - LN)^{-1} D_I\right]^2 + \left[\sum_j (M - LN)^{-1} L D_O\right]^2}. \tag{34}$$

In any case, Kostya's procedure should be checked against a more extensive use of eq. (32).

2.3.2 Glenn

At present I have no understanding of how Glenn assigns errors.

2.4 Some Details

2.4.1 Kostya

Kostya solves eq. (24) by an iterative procedure in which each iteration begins with a hypothesis for the spectrum F_i that we are trying to reconstruct in ECAL. The initial hypothesis is that $F_i = D_{I,i}$, the observed spectrum in the inner columns. The procedure is declared to have converged after two iterations.

A. Calculation of Matrices M and N

Corresponding to a set of F_i we need a continuous function $f(y)$ so that the integrals (9) can be performed and the coefficients M_{ij} read off according to eq. (10). To make it easy to do the integrals analytically, Kostya chose to approximate $f(y)$ as a polyline. Further, it is useful that the endpoints of the line segments are at row boundaries. Then $f(y)$ over row i is characterized by the central value F_i and a slope m_i. See Figure 5.

Kostya's analysis applies to the top four rows of ECAL, so we must determine four slopes m_i. However, the slopes of the polyline through the four F_i is not unique until one additional point is fixed. This is taken to be the intercept of the polyline at the boundary between rows 4 and 5. That intercept is determined by a linear extrapolation of values D_5 and D_6 to the 4-5 boundary. If the extrapolated intercept is negative an intercept of zero is used.

For F_i that are monotonically decreasing and always positive the slopes m_i are always in the range $-2 < m_i < 0$.

Apparently a check was made that the polyline $f(y)$ remains positive over all four rows and some action was foreseen if this test failed. In practice there were no cases in which the polyline went negative.

For any the polyline $f(y)$ the integrals (9) can be carried out using the kernels K_I and K_O summed over ECAL longitudinal segments 1-3. When the results are written in the form

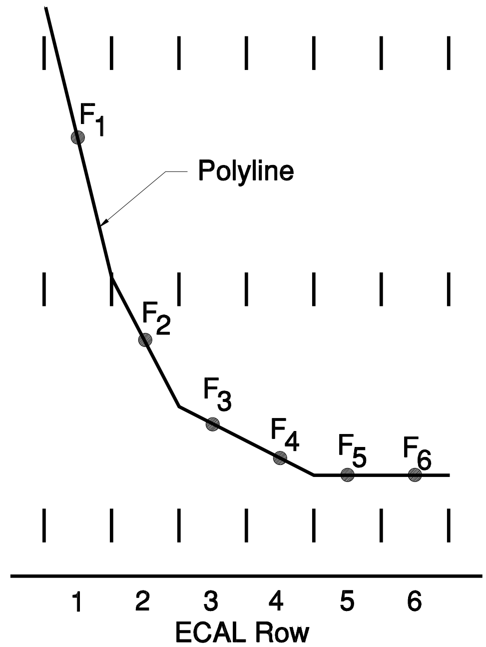

Figure 5: Construction of a polyline from a hypothesis to the spectrum F_i in ECAL.

(10) the matrix M_{ij} does not depend directly on the F_i, but only on the slopes m_i in the simple form

$$M_{ij} = \begin{bmatrix} 0.77 & 0.10 - 0.024m_2 & 0.011 - 0.0015m_3 & 0.0021 - 0.00027m_4 \\ 0.10 + 0.024m_1 & 0.77 & 0.10 - 0.024m_3 & 0.011 - 0.0015m_4 \\ 0.011 + 0.0015m_1 & 0.10 + 0.024m_2 & 0.77 & 0.10 - 0.024m_4 \\ 0.0021 + 0.00027m_1 & 0.011 + 0.0015m_2 & 0.10 + 0.024m_3 & 0.77 \end{bmatrix}. \tag{35}$$

The diagonal element M_{ii} tell us that on average 77% of an electron's energy is deposited in the inner columns of the same ECAL row that it enters. Looking at column 2 of the matrix, we see that if the Compton spectrum were flat ($m_2 = 0$) then 10% of an electrons energy would be deposited in the row above and 10% in the row below the one it entered. For a nonuniform spectrum with $m_2 < 0$ the electron more probably enters the top of the row and so more energy leaks into the row above than the row below, as described by M_{13} and M_{32} for an electron entering row 2, *etc.*

We can also calculate the energy deposited in the outer columns by Compton electrons entering the inner columns with a spectrum $f(y)$ approximated by a polyline. The result is described by matrix N introduced in eq. (19):

$$N_{ij} = \begin{bmatrix} 0.025 & 0.014 - 0.0011m_2 & 0.0055 - 0.00043m_3 & 0.0021 - 0.00017m_4 \\ 0.014 + 0.0011m_1 & 0.025 & 0.014 - 0.0011m_3 & 0.0055 - 0.00043m_4 \\ 0.0055 + 0.00043m_1 & 0.014 + 0.0011m_2 & 0.025 & 0.014 - 0.0011m_4 \\ 0.0021 + 0.00017m_1 & 0.0055 + 0.00043m_2 & 0.014 + 0.0011m_3 & 0.025 \end{bmatrix}. \quad (36)$$

We see from M_{ij} that over 98% of the energy is accounted for, taking all the slopes to be zero and summing over a column. This corresponds to the normalization convention (2). Similarly, summing over a column in matrix N we find 6% of the energy has leaked into the outer columns, corresponding to (3).

In practice, Kostya makes adjustments to the $i1$ elements of (35) and (36) to account for energy leaking down into ECAL from the showers due to Compton electrons that hit tungsten plate above it. Addition adjustments are made to bring the results into better agreement with the calibration data. The revised matrices are

$$M_{ij} = \begin{bmatrix} 0.87 - 0.081m_1 & 0.089 - 0.016m_2 & 0.0083 - 0.0007m_3 & 0.0035 - 0.0007m_4 \\ 0.097 + 0.0077m_1 & 0.789 & 0.089 - 0.016m_3 & 0.0083 - 0.0007m_4 \\ 0.0104 - 0.0024m_1 & 0.089 + 0.016m_2 & 0.789 & 0.089 - 0.016m_4 \\ 0.0056 - 0.0014m_1 & 0.0083 + 0.0007m_2 & 0.089 + 0.016m_3 & 0.789 \end{bmatrix}, \quad (37)$$

and

$$N_{ij} = \begin{bmatrix} 0.026 - 0.0083m_1 & 0.010 - 0.0010m_2 & 0.0055 - 0.00043m_3 & 0.0021 - 0.00017m_4 \\ 0.014 + 0.0011m_1 & 0.025 & 0.014 - 0.0011m_3 & 0.0055 - 0.00043m_4 \\ 0.0055 + 0.00043m_1 & 0.014 + 0.0011m_2 & 0.025 & 0.014 - 0.0011m_4 \\ 0.0021 + 0.00017m_1 & 0.0055 + 0.00043m_2 & 0.014 + 0.0011m_3 & 0.025 \end{bmatrix}. \quad (38)$$

(Some elements of N not yet right...)

2.4.2 Glenn

A major step in Glenn's approach is the minimization of the χ^2 given in eq. (26) to find the reconstruction matrix R. For this the 'errors' or tolerances σ_{ik} and σ' must be stated.

The tolerance function σ_{ik} is shown in Fig. 6. Recall that the aperture function $g_i(y)$ is unity for ± 8 mm about the vertical center of a row and zero elsewhere. Glenn chose to enforce a tighter tolerance on the aperture function where it should be zero than where it should be one, and graded the tolerance in the regions 7-10 mm from the row center for best results.

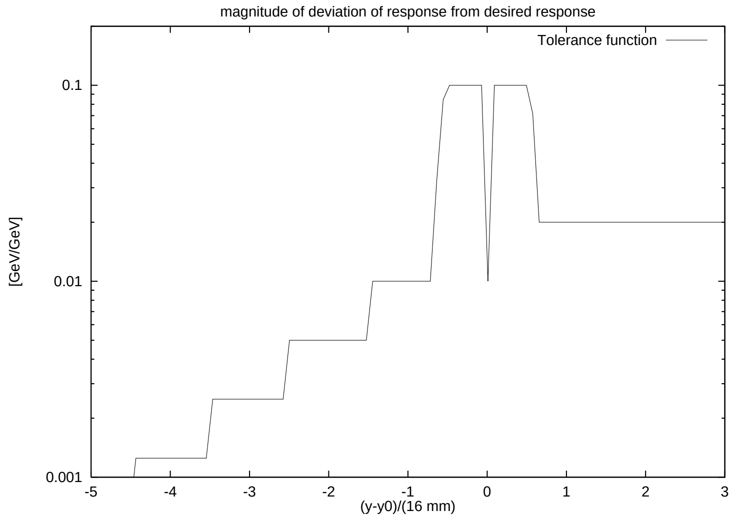

Figure 6: The tolerance function σ_{ik} as a function of vertical distance from the center of a row.

Once matrix R has been calculated we obtain a measure of its validity by calculating the aperture functions via eq. (13). Figure 7 shows the resulting aperture functions for the top four rows of ECAL on a log scale (Fig. 4 shows the same functions on a linear scale).

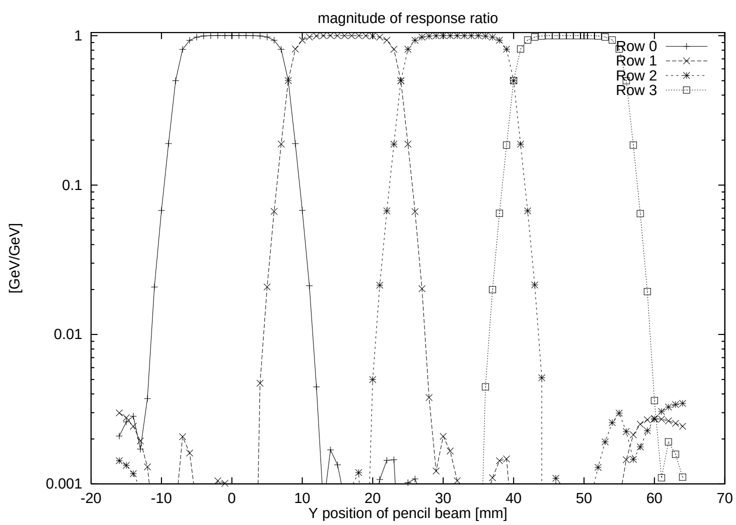

Figure 7: The aperture functions defined by eq. (13) for the top four rows of ECAL.

(I would like to understand more about tolerance σ' and whether there is any measure of how well the background subtraction works.

Figure 8 was provided by Glenn, but I need him to explain it.)

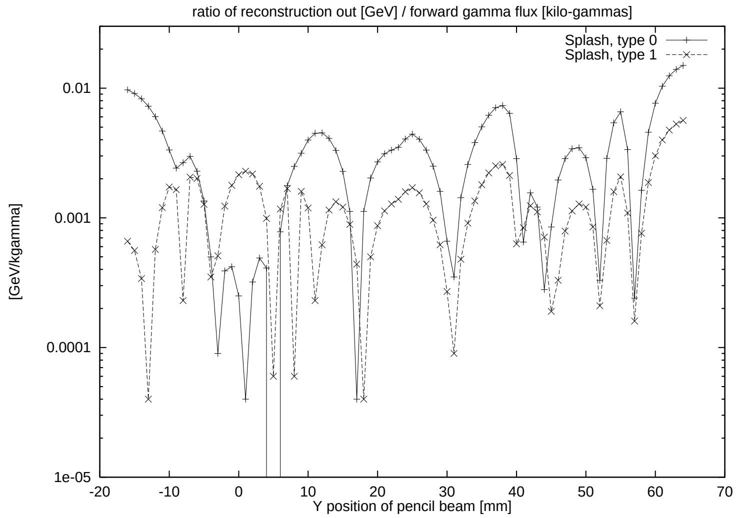

Figure 8: ???

3 Comparison of Numerical Results

Figures 9-16 were recently made by Kostya to compare the results of his and Glenn's analyses. They were extracted from Kostya's Home Page. I believe essentially all circularly polarized nonlinear Compton data from March '95 is summarized in the plots.

A few remarks:

1. Figures 9 and 13 compare $F_{i,Kostya}$ and $F_{i,Glenn}$ for the top four rows of ECAL. In rows 1 and 2 there seem to be several subgroups of data where within each subgroup the agreement between Glenn and Kostya is remarkable. However, there seems to be different normalizations between Glenn and Kostya. clearly it will be interested to subdivide the data according to run number or ECAL positions to see if the subgroups are correlated with this.

2. Results from row 4 show some correlation between Glenn and Kostya – but the correlation is so weak that we should examine carefully whether we retain this row in the final results.

3. Figures 11-12 and 15-16 shows that the error estimates of Glenn and Kostya are similar in rows 1 and 2, but with Glenn assigning somewhat smaller errors in row 3, and assigning errors much smaller than Kostya in row 4. Judging from the correlation plots, Figs. 9 and 13, I infer that the larger error estimates of Kostya are more realistic.

4. The error correlation plots, Figs. 10 and 14 suggest that the analysis is unreliable in case of very small signals in any row. This should be looked into further.

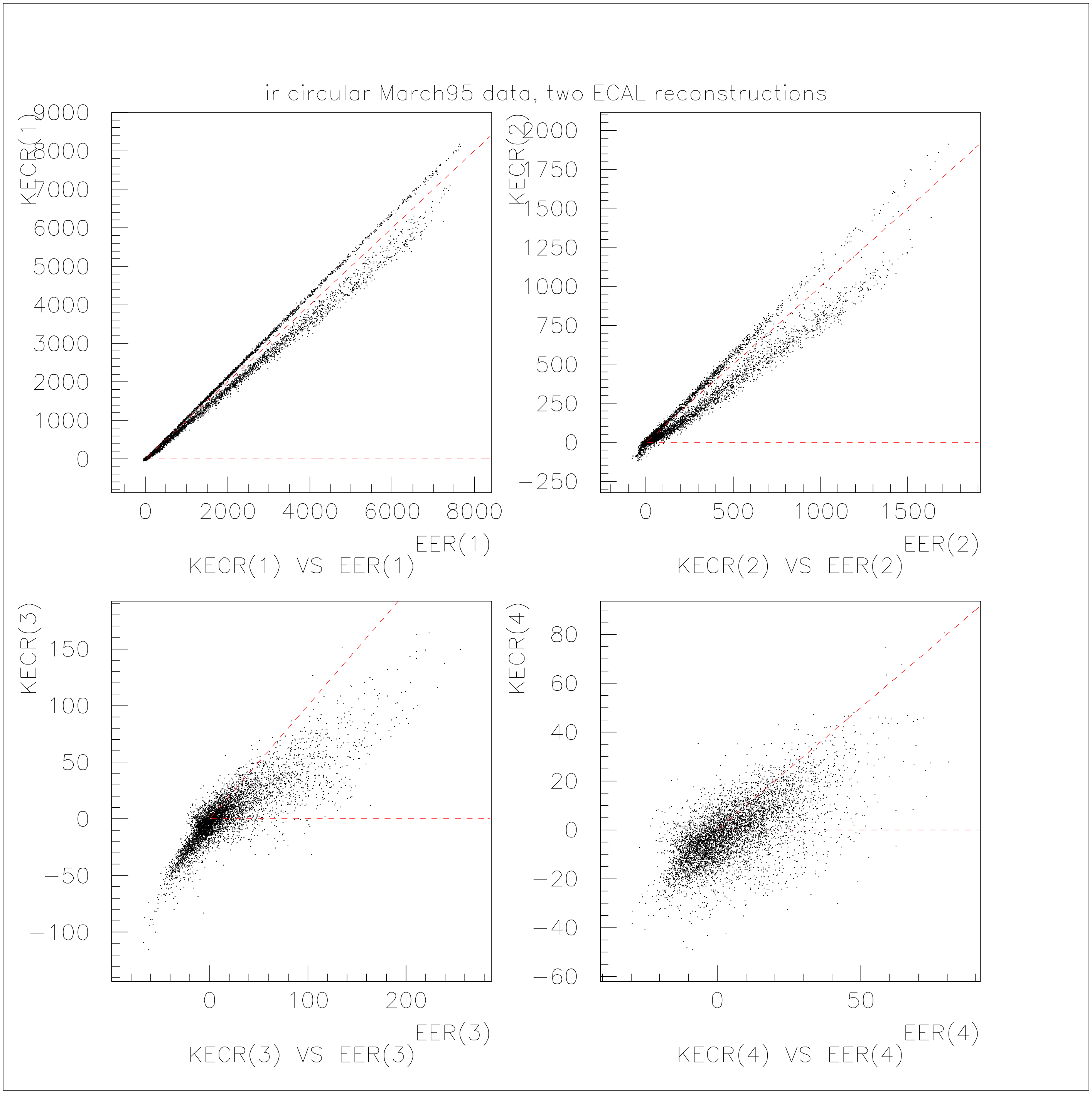

Figure 9: Comparison of results from Glenn and Kostya for infrared laser data.

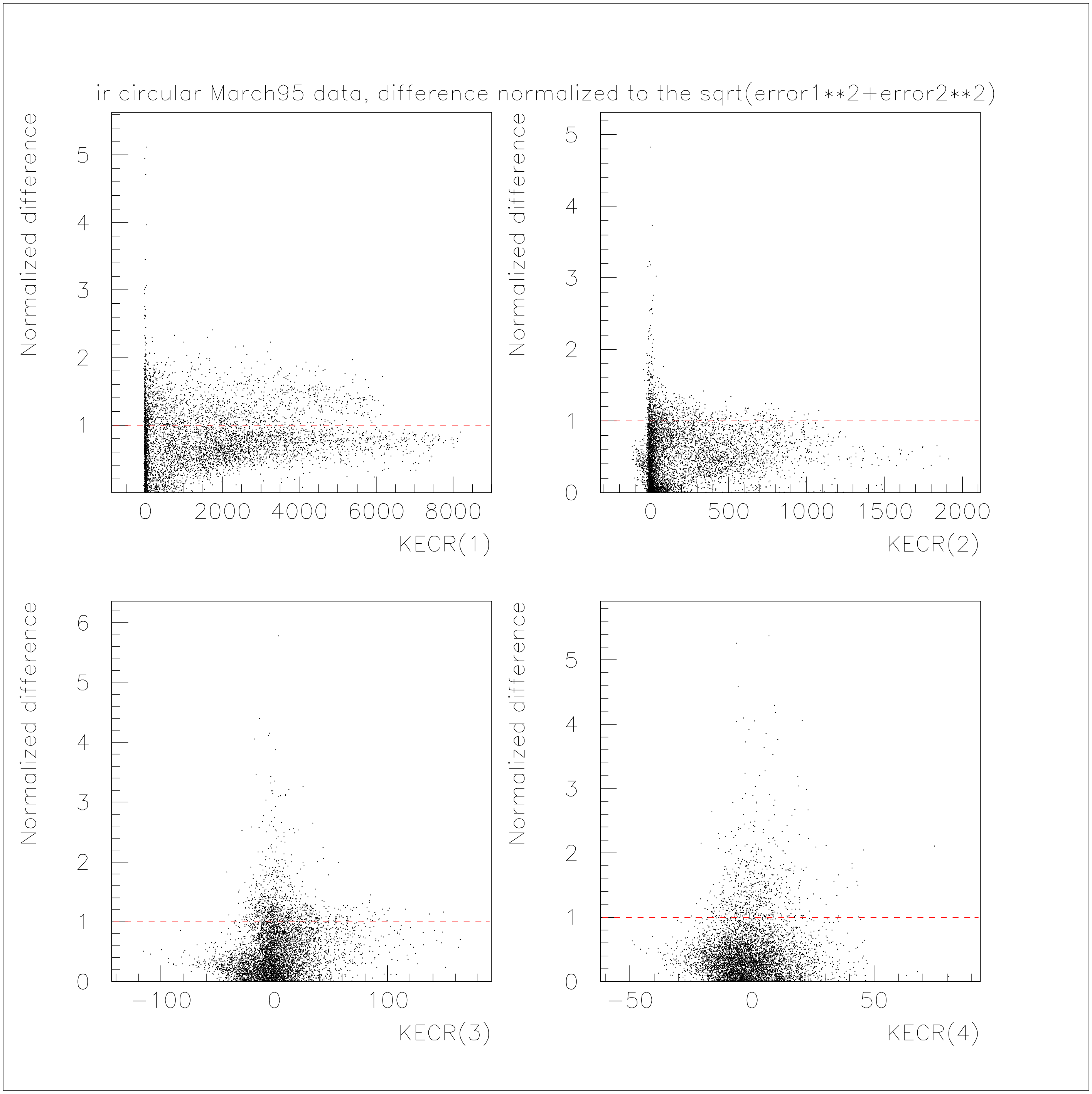

Figure 10: Comparison of results from Glenn and Kostya for infrared laser data.

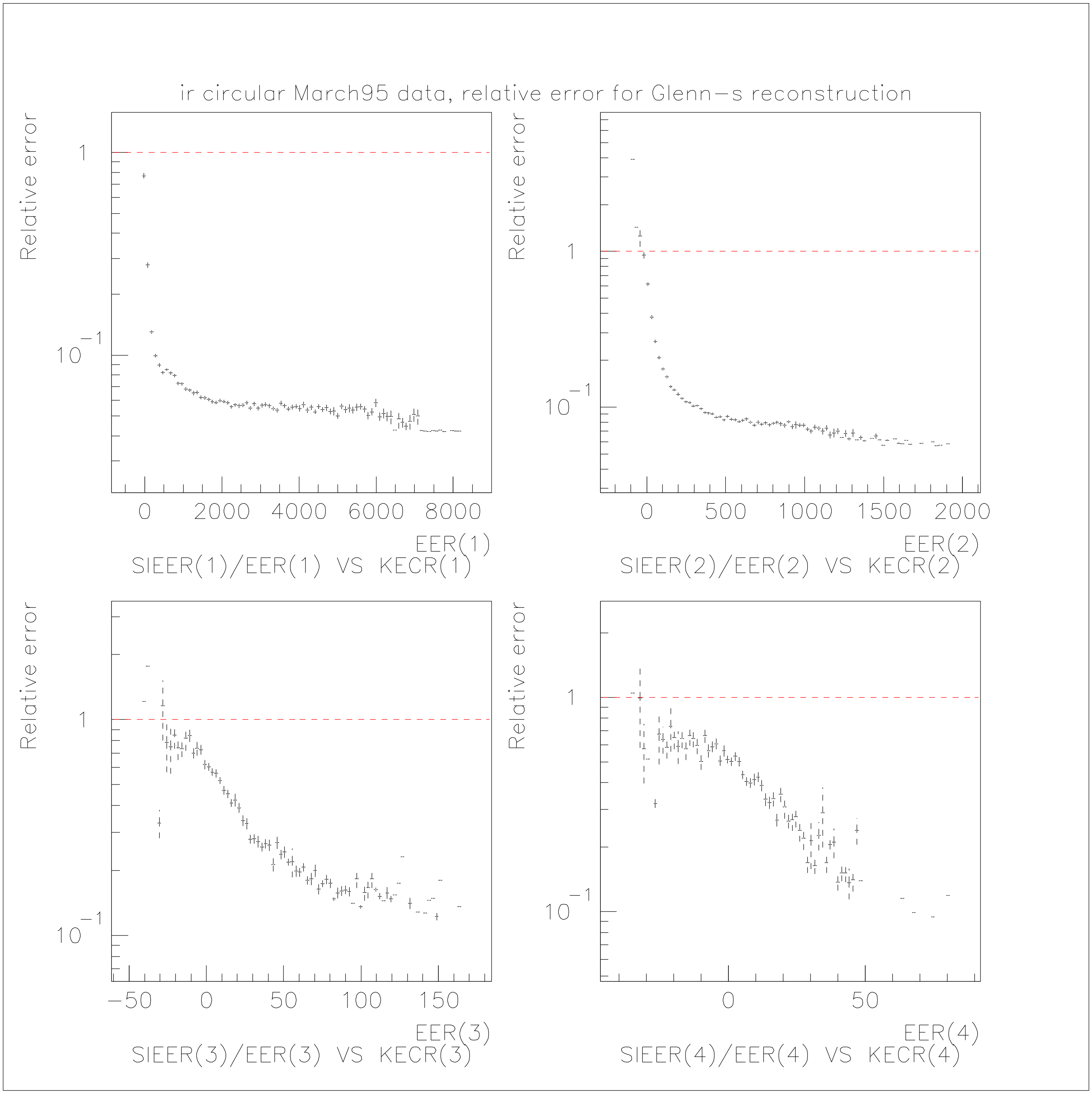

Figure 11: Comparison of results from Glenn and Kostya for infrared laser data.

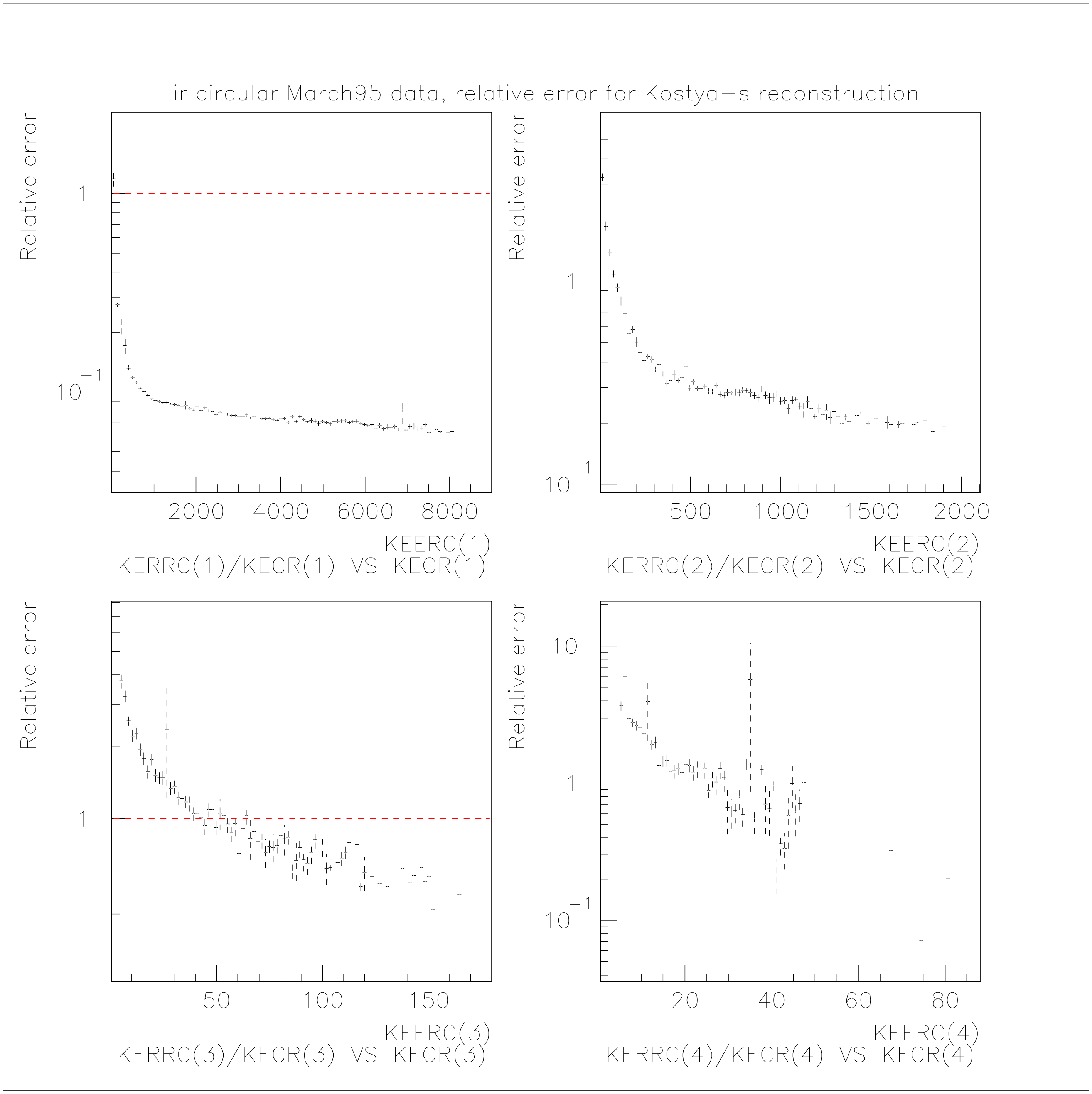

Figure 12: Comparison of results from Glenn and Kostya for infrared laser data.

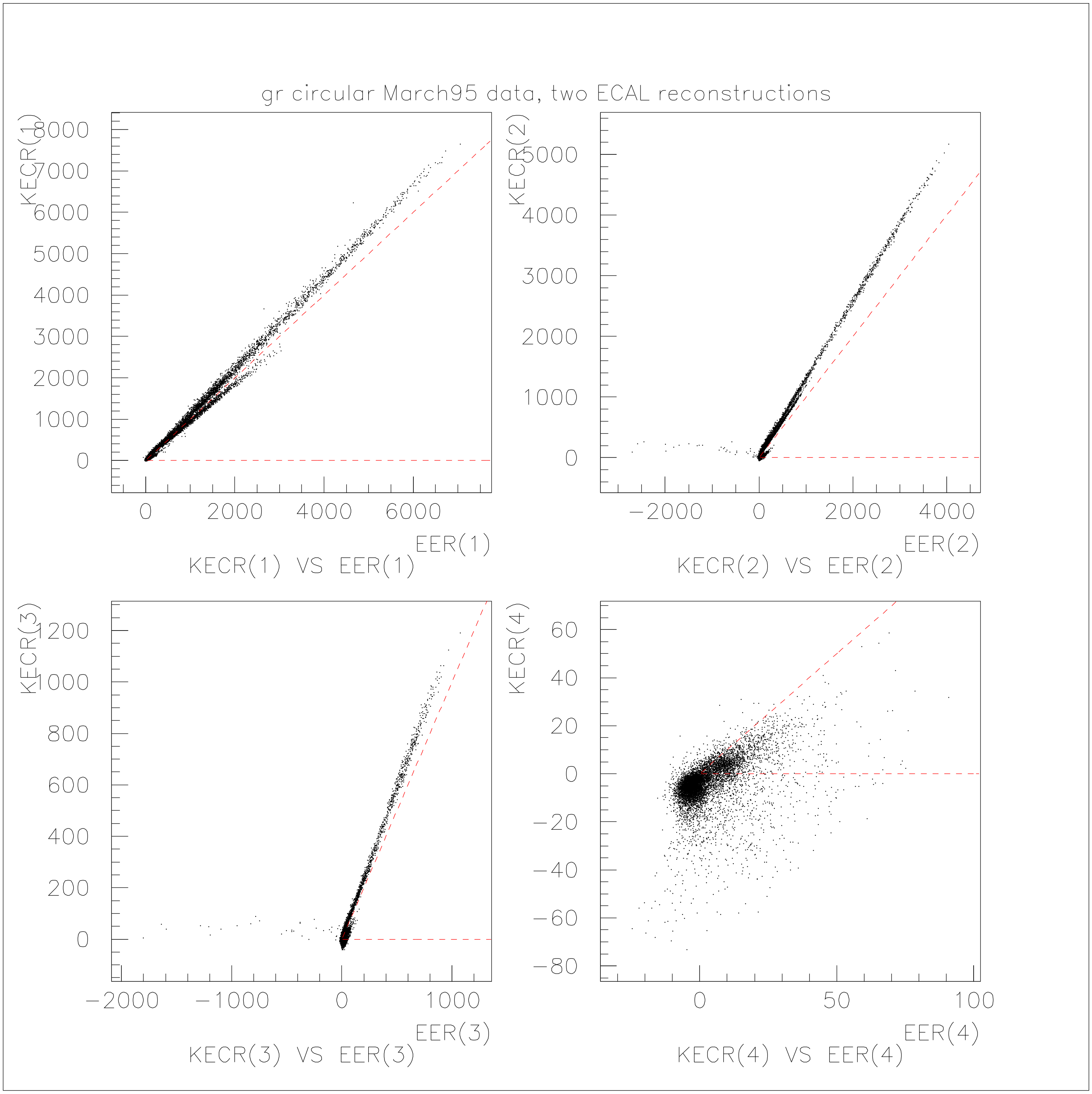

Figure 13: Comparison of results from Glenn and Kostya for green laser data.

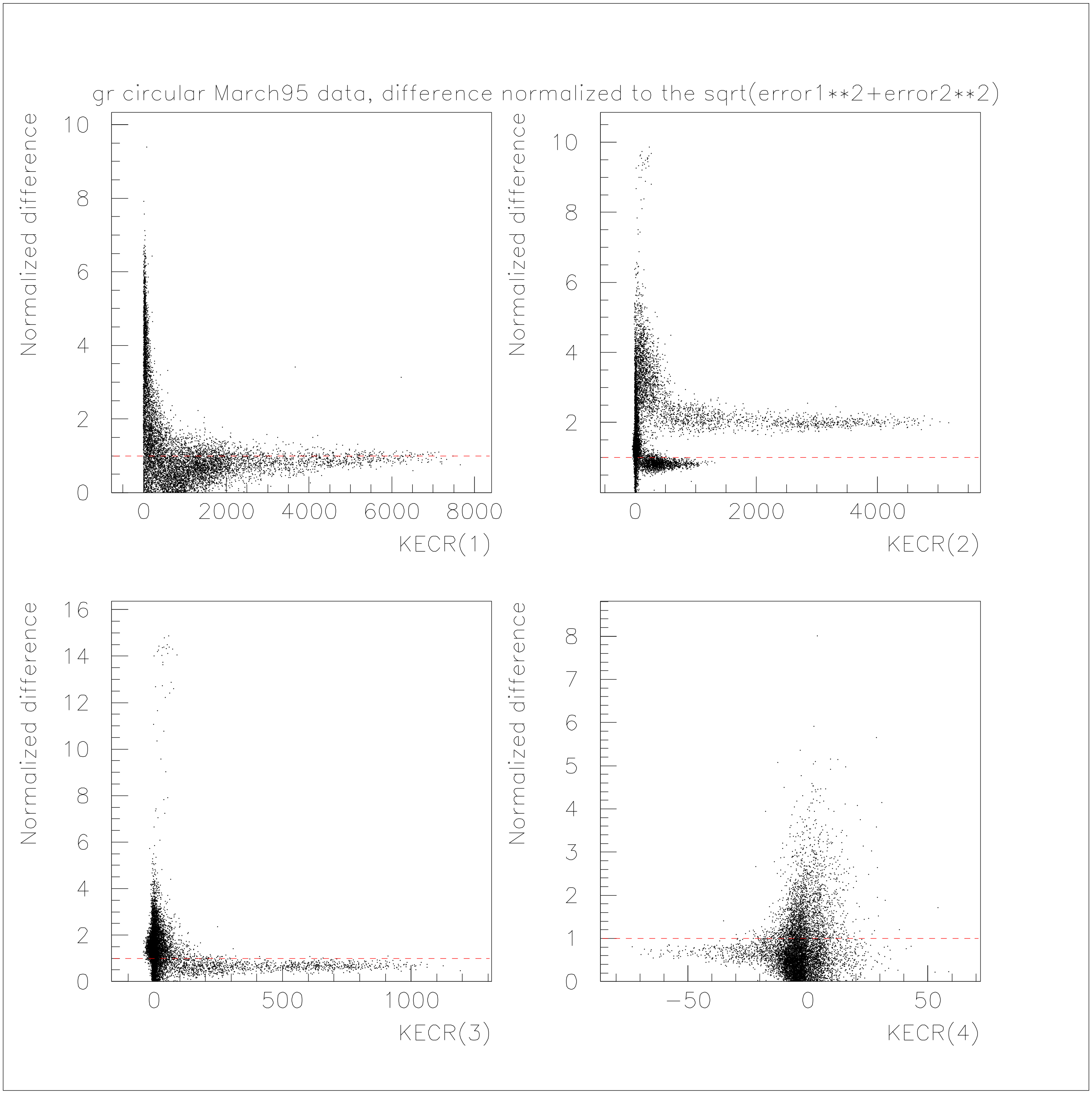

Figure 14: Comparison of results from Glenn and Kostya for green laser data.

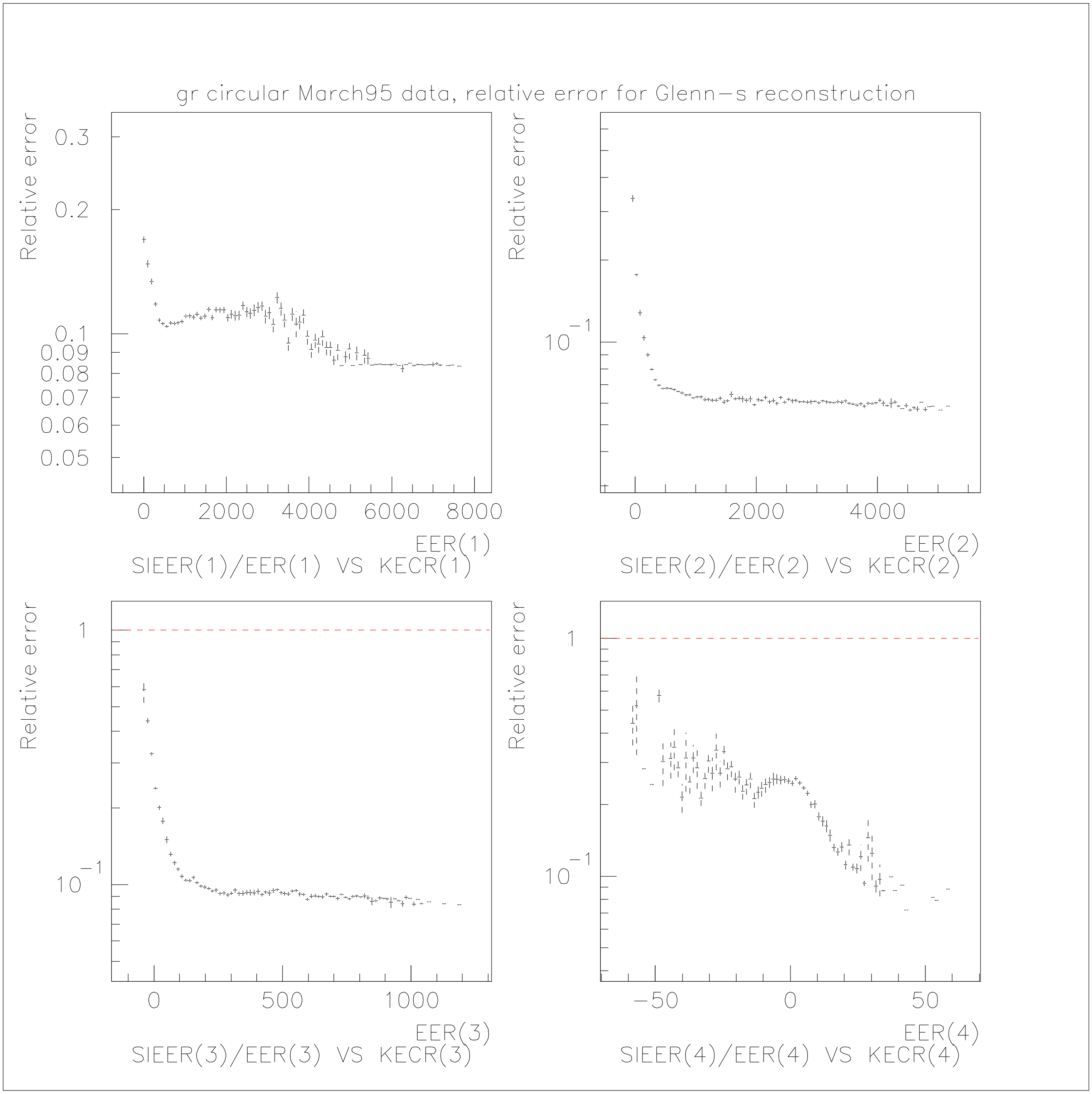

Figure 15: Comparison of results from Glenn and Kostya for green laser data.

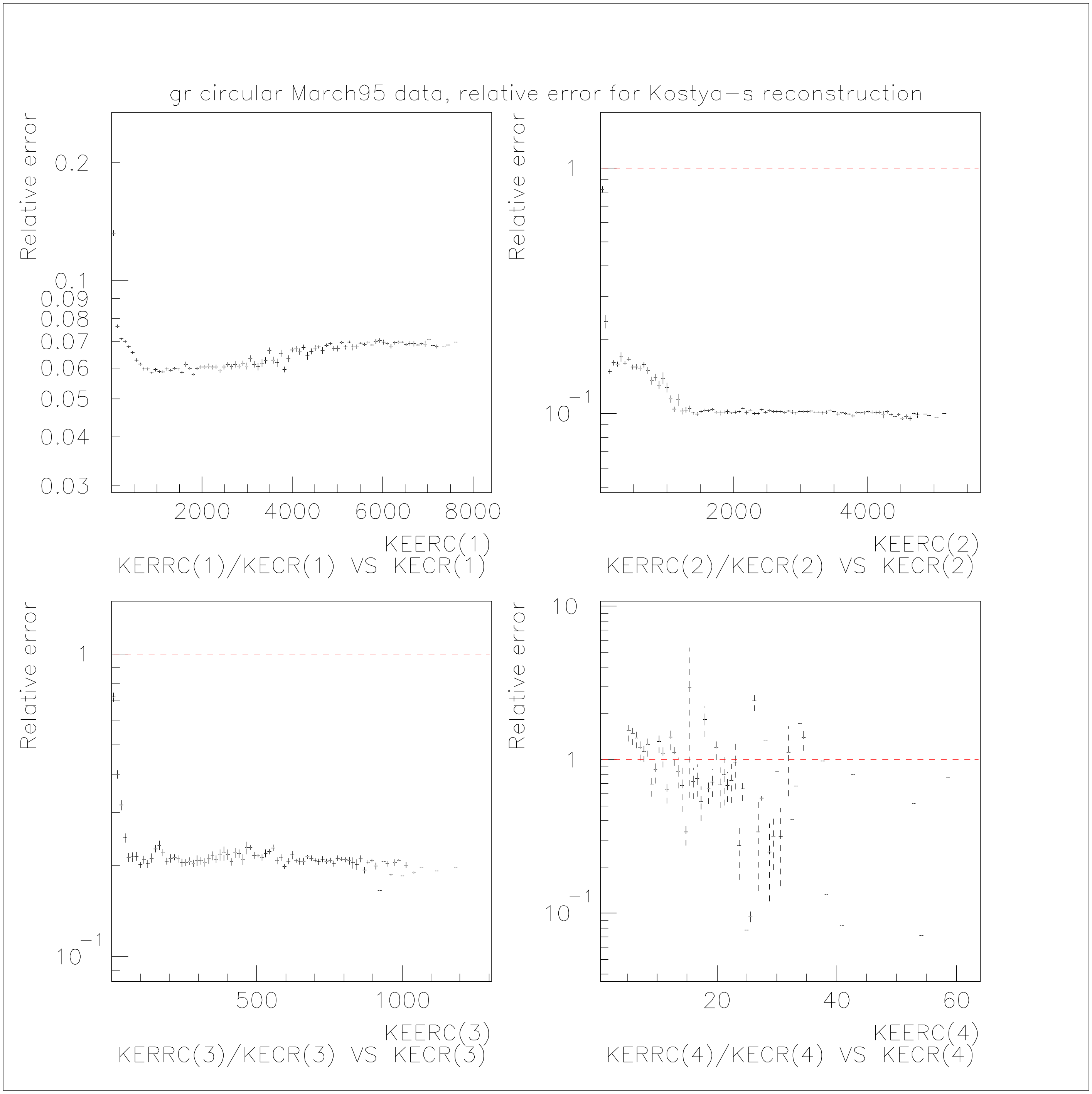

Figure 16: Comparison of results from Glenn and Kostya for green laser data.